Swine acute diarrhea syndrome coronavirus replication in primary human cells reveals potential susceptibility to infection

Caitlin E. Edwards[a], Boyd L. Yount[a], Rachel L. Graham[a], Sarah R. Leist[a], Yixuan J. Hou[a], Kenneth H. Dinnon III[b], Amy C. Sims[c], Jesica Swanstrom[a], Kendra Gully[d], Trevor D. Scobey[a], Michelle R. Cooley[a], Caroline G. Currie[a], Scott H. Randell[e], and Ralph S. Baric[a,b,f,1]

[a]Department of Epidemiology, University of North Carolina at Chapel Hill, Chapel Hill, NC 27599; [b]Department of Microbiology and Immunology, University of North Carolina at Chapel Hill, Chapel Hill, NC 27599; [c]Chemical and Biological Signatures Division, Pacific Northwest National Laboratory, Richland, WA 99354; [d]Department of Comparative Medicine, University of North Carolina at Chapel Hill, Chapel Hill, NC 27599; [e]Marsico Lung Institute, University of North Carolina at Chapel Hill, Chapel Hill, NC 27599; and [f]Rapidly Emerging Antiviral Drug Discovery Initiative, University of North Carolina, Chapel Hill, NC 27599

Edited by Peter Daszak, EcoHealth Alliance, New York, NY, and accepted by Editorial Board Member Diane E. Griffin August 18, 2020 (received for review January 22, 2020)

Zoonotic coronaviruses represent an ongoing threat, yet the myriads of circulating animal viruses complicate the identification of higher-risk isolates that threaten human health. Swine acute diarrhea syndrome coronavirus (SADS-CoV) is a newly discovered, highly pathogenic virus that likely evolved from closely related HKU2 bat coronaviruses, circulating in *Rhinolophus* spp. bats in China and elsewhere. As coronaviruses cause severe economic losses in the pork industry and swine are key intermediate hosts of human disease outbreaks, we synthetically resurrected a recombinant virus (rSADS-CoV) as well as a derivative encoding tomato red fluorescent protein (tRFP) in place of ORF3. rSADS-CoV replicated efficiently in a variety of continuous animal and primate cell lines, including human liver and rectal carcinoma cell lines. Of concern, rSADS-CoV also replicated efficiently in several different primary human lung cell types, as well as primary human intestinal cells. rSADS-CoV did not use human coronavirus ACE-2, DPP4, or CD13 receptors for docking and entry. Contemporary human donor sera neutralized the group I human coronavirus NL63, but not rSADS-CoV, suggesting limited human group I coronavirus cross protective herd immunity. Importantly, remdesivir, a broad-spectrum nucleoside analog that is effective against other group 1 and 2 coronaviruses, efficiently blocked rSADS-CoV replication in vitro. rSADS-CoV demonstrated little, if any, replicative capacity in either immune-competent or immunodeficient mice, indicating a critical need for improved animal models. Efficient growth in primary human lung and intestinal cells implicate SADS-CoV as a potential higher-risk emerging coronavirus pathogen that could negatively impact the global economy and human health.

SADS | coronavirus | One Health | emerging infectious disease

One Health recognizes that human, animal, and environmental health are tightly interconnected (1). In the 21st century, three novel human and three novel swine coronaviruses (CoVs) have emerged suddenly and spread globally, demonstrating a critical need for strategies that identify higher risk zoonotic coronaviruses (2). Contemporary human coronaviruses include four isolates (e.g., HCoV NL63, HCoV 229E, and HCoV OC43, HCoV HKU1) that reside within the group 1b and group 2a subgroups, respectively, and cause significant upper and lower respiratory infections in children and adults (3). These viruses likely originated from strains in bats, rodents, and bovine before the beginning of the 20th century (3). More recently, highly pathogenic human coronaviruses include the betacoronavirus subgenra Sarbecovirus severe acute respiratory syndrome coronavirus (SARS-CoV) strains that emerged in China in 2003 and the Merbecovirus Middle East respiratory syndrome coronavirus (MERS-CoV) strains that emerged in the Middle East in 2012. SARS-CoV and MERS-CoV cause an atypical pneumonia that rapidly progresses to acute respiratory distress syndrome, with fatalities rates of 10% and 35%, respectively (4, 5). While the MERS-CoV outbreak is still ongoing throughout the Middle East and Sub-Saharan Africa, heterogeneous SARS- and MERS-like CoVs with human epidemic potential are circulating in bat species in Southeast Asia and elsewhere (6–8). As these data forecast, a new Sarbecovirus recently emerged in Wuhan, China in 2019 (SARS-CoV-2). As of September 2020, the rapidly expanding outbreak has surpassed 31 million cases, many of whom have progressed to respiratory failure, resulting in more than 972,000 deaths worldwide in the last 9 mo (see The Johns Hopkins University Dashboard, https://gisanddata.maps.arcgis.com/apps/opsdashboard/index.html#/bda7594740fd40299423467b48e9ecf6) (9). Clearly, the cross-species transmission potential of zoonotic CoVs to humans and other important domesticated species remains high as global pathogens of concern (2, 10).

Over the past 80 y, several novel coronaviruses have caused extensive outbreaks and economic losses in swine, including transmissible gastroenteritis virus (TGEV), porcine respiratory coronavirus (PRCV), porcine epidemic diarrhea coronavirus (PEDV), porcine hemagglutinating encephalomyelitis virus (PHEV), and porcine deltacoronavirus (PDCoV) (11–14). Between October 2016 and 2019,

Significance

The emergence of new human and animal coronaviruses demand novel strategies that characterize the threat potential of newly discovered zoonotic strains. We synthetically recovered recombinant wild-type and derivative swine acute diarrhea syndrome coronaviruses (SADS-CoVs) that express indicator genes and characterized their growth, macromolecular biosynthesis, and replication efficiency in a variety of mammalian cell lines, including primary human cells. The data demonstrate that SADS-CoV has a broad host range and has inherent potential to disseminate between animal and human hosts, perhaps using swine as an intermediate species.

Author contributions: C.E.E., B.L.Y., S.R.L., and R.S.B. designed research; C.E.E., B.L.Y., S.R.L., Y.J.H., A.C.S., J.S., K.G., T.D.S., M.R.C., and C.G.C. performed research; S.H.R. contributed new reagents/analytic tools; C.E.E., B.L.Y., R.L.G., S.R.L., K.H.D., A.C.S., J.S., and R.S.B. analyzed data; and C.E.E. and R.S.B. wrote the paper.

The authors declare no competing interest.

This article is a PNAS Direct Submission. P.D. is a guest editor invited by the Editorial Board.

[1]To whom correspondence may be addressed. Email: rbaric@email.unc.edu.

This article contains supporting information online at https://www.pnas.org/lookup/suppl/doi:10.1073/pnas.2001046117/-/DCSupplemental.

First published October 12, 2020.

several novel coronavirus outbreaks were described in swine herds throughout China. Infection with the novel swine acute diarrhea syndrome coronavirus (SADS-CoV) was associated with acute diarrhea and vomiting with 90% mortality rates in piglets less than 5 d of age (10, 15–17). SADS-CoV is an alphacoronavirus most closely related to bat coronavirus HKU2, while also being distantly related to other coronaviruses, such as HCoV 229E, HCoV NL63, and swine coronavirus PEDV (15). *Rhinolophus* spp. bats in the vicinity of local outbreaks had viruses (HKU2) with high sequence similarity to SADS-CoV strains, demonstrating that SADS-CoV likely originated from bats (10). The recent and rapid global dissemination of highly pathogenic variants of PEDV and PDCoV highlights the critical One Health threat associated with a newly emerged swine coronavirus (18, 19), and demonstrates a need for resources to understand the virus and its pathogenic potential in mammals.

The goal of this study was to evaluate human susceptibility for SADS-CoV cross-species transmission and replication. To address this question, we synthesized a full-length infectious clone and recovered wild-type and derivative recombinant (r)SADS-CoV that expresses tomato red fluorescent protein (rSADS-CoV tRFP). We used these viruses to study virus replication, transcription programs, and gene expression in vitro. We also demonstrated that SADS-CoV replicated efficiently in primary human cells derived from both the lung and intestine, highlighting an intrinsic potential for cross-species transmission and human susceptibility to infection. Although wild-type and IFN receptor (IFNR)-immunodeficient mice were not susceptible, we demonstrated the availability of a small-molecule inhibitor that efficiently block SADS-CoV replication in vitro. While revealing the threat potential of SADS-CoV to humans and the global community, the reagents and models provide a critical infrastructure to study the molecular and evolutionary programs that promote virus cross-species transmission while providing for potential intervention strategies designed to control the pandemic spread of SADS-CoV in swine and potentially humans.

Results

Assembly of SADS-CoV Full-Length cDNAs. SADS-CoV likely emerged after multiple independent virus introductions from heterologous bat coronavirus strains circulating in bat populations into swine in China (10). We focused on the prototype SADS-CoV isolate (GenBank, accession no. MG557844) (Fig. 1*A* and *SI Appendix*, Fig. S7). In developing a SADS-CoV infectious clone, we synthesized a panel of contiguous cDNAs spanning the entire SADS-CoV genome that could be restricted with endonucleases and ligated in vitro to assemble genome-length cDNA (Fig. 1*B*) (20, 21). The individual cDNAs were linked by unique restriction endonuclease sites between neighboring fragments, namely BsmBI, SapI, and BglI. BsmBI and SapI sites were introduced to each fragment externally in the plasmid sequence and were lost following digestion and ligation (22), whereas the BglI site is internal to the corresponding fragments (Fig. 1*C*). The SADS-CoV A fragment contains a T7 promoter at the 5′ end, and the SADS-CoV F fragments terminates in a poly-A track at the 3′ end followed by a NotI restriction site. Each fragment (SADS-CoV A–F) was stable in *Escherichia coli* and allowed for systematic and directional assembly of the full-length SADS-CoV cDNA.

Following electroporation of recombinant rSADS-CoV genome-length transcripts into Vero CCL-81 cells in combination with SADS-CoV nucleocapsid (N) gene transcripts to enhance infectivity (22–24), rSADS-CoV virus replication was demonstrated by the presence of subgenomic length leader-containing RNA transcripts in cultures at 24 and 48 h postinfection (hpi). Moreover, wild-type virus produced both cytopathic effects and plaques in culture and could be serially passaged in vitro (*SI Appendix*, Fig. S1). Importantly and like several other zoonotic coronaviruses (25), one-step growth curves demonstrated efficient virus growth in swine LLC-PK1 and primate Vero CCL-81 kidney cultures with virus titers exceeding 10^6 plaque forming units (PFU)/mL, in the presence, but not absence, of low levels of trypsin (10 μg/mL) (Fig. 2 *A* and *B*).

Recombinant viruses that encode indicator genes provide tools to study virus host range, species specificity, and sensitivity to small-molecule inhibitors. To generate recombinant SADS-CoV indicator viruses, we replaced the accessory ORF encoding nonstructural protein 3a (ORF3a) with the gene encoding tRFP, noting that many downstream ORFs encode luxury functions in the Coronaviridae, including the ORF3 proteins of PEDV and HCoV NL63 (Fig. 1*D*) (23, 26, 27). Integrating tRFP into the SADS-CoV genome (rSADS-CoV tRFP) allows for real-time visualization of virus replication via fluorescence microscopy in living cells, providing a strong marker for productive virus infection, subgenomic transcription, and replication. Despite the loss of ORF3a, rSADS-CoV tRFP replicated to titers similar to wild-type rSADS-CoV, approaching ~10^6 PFU/mL, in LLC-PK1 cells and Vero CCL-81 cells following a single-cycle growth curve over a 48-h time course (Fig. 2 *A* and *B*). tRFP expression observed under a fluorescent microscope demonstrated productive infections of LLC-PK1 and Vero CCL-81 cells with SADS-CoV (Fig. 2*D*). Additionally, Northern blot analysis was utilized to detect the predicted mRNAs that should be expressed during SADS-CoV infection in vitro (Fig. 2*E*). These data demonstrate that ORF3 is likely not essential for efficient virus replication in vitro.

Alphaviruses like the highly attenuated, nonselect Venezuelan equine encephalitis virus strain 3526 (VEE 3526) have been engineered as replicons to express high concentrations of foreign transgene proteins in cell culture and in animals (28). To evaluate SADS-CoV structural protein synthesis following infection, we produced VEE 3526 replicon particles (VRP) expressing the SADS-CoV N and spike (S) genes. Using mouse antisera from mice infected with the VEE VRP expressing the SADS-CoV N gene, we demonstrated extensive N protein expression in LLC-PK1 cells via Western blotting (Fig. 2*C*). Additionally, CCL-81 cells infected with rSADS-CoV tRFP were stained using both N and S antisera from vaccinated mice and images observed via immunoflourescence assay (Fig. 3 *D* and *E*). Both N and S proteins are clearly evident in the infected cultures.

SADS-CoV Species Specificity. Using the rSADS-CoV tRFP indicator virus, we examined recombinant virus growth in different hosts, including immortalized monkey, pig, cat, and human cells. At 48 hpi, rSADS-CoV tRFP produced robust tRFP expression that was detected in African green monkey Vero CCL-81, swine LLC-PK1, and feline AK-D lung cells (Figs. 2*D* and 3*A*). Vero CCL-81 and LLC-PK1 cells also displayed increased tRFP fluorescence in the presence of trypsin, which was required for adequate viral propagation (*SI Appendix*, Fig. S2). At 48 hpi, viral infections were also detected in human cells via red fluorescence, including liver (Huh7.5), intestine (CaCo2), stomach-intestine (ST-INT), and colorectal tumor cells (HRT) (Fig. 3*A*), including limited overlap with cell lines reported by others (29). Importantly, rSADS-CoV tRFP growth in Huh7.5 cells was robust even in the absence of exogenous trypsin treatment, replicating to titers of >10^5 PFU/mL (Fig. 3*B*).

Immortalized cells are often derived from cancers or encode aberrant numbers of chromosomes, including extensive deletions and duplications, resulting in the loss of many key innate immune and other antiviral genes (30–32). Consequently, evaluating zoonotic coronavirus infection potential and growth in primary cells derived from humans provides a more realistic assessment of potential human susceptibility (7, 8, 33). Importantly, primary human lung cells, including microvascular endothelial cells (MVE), fibroblasts (FB), human nasal epithelial (HNE), and human airway epithelial cells (HAE) were all susceptible to productive SADS-CoV infection (Fig. 4 *A*–*C* and *SI Appendix*, Fig. S4*A*). While SADS-CoV replicated most efficiently in MVE and FB cultures,

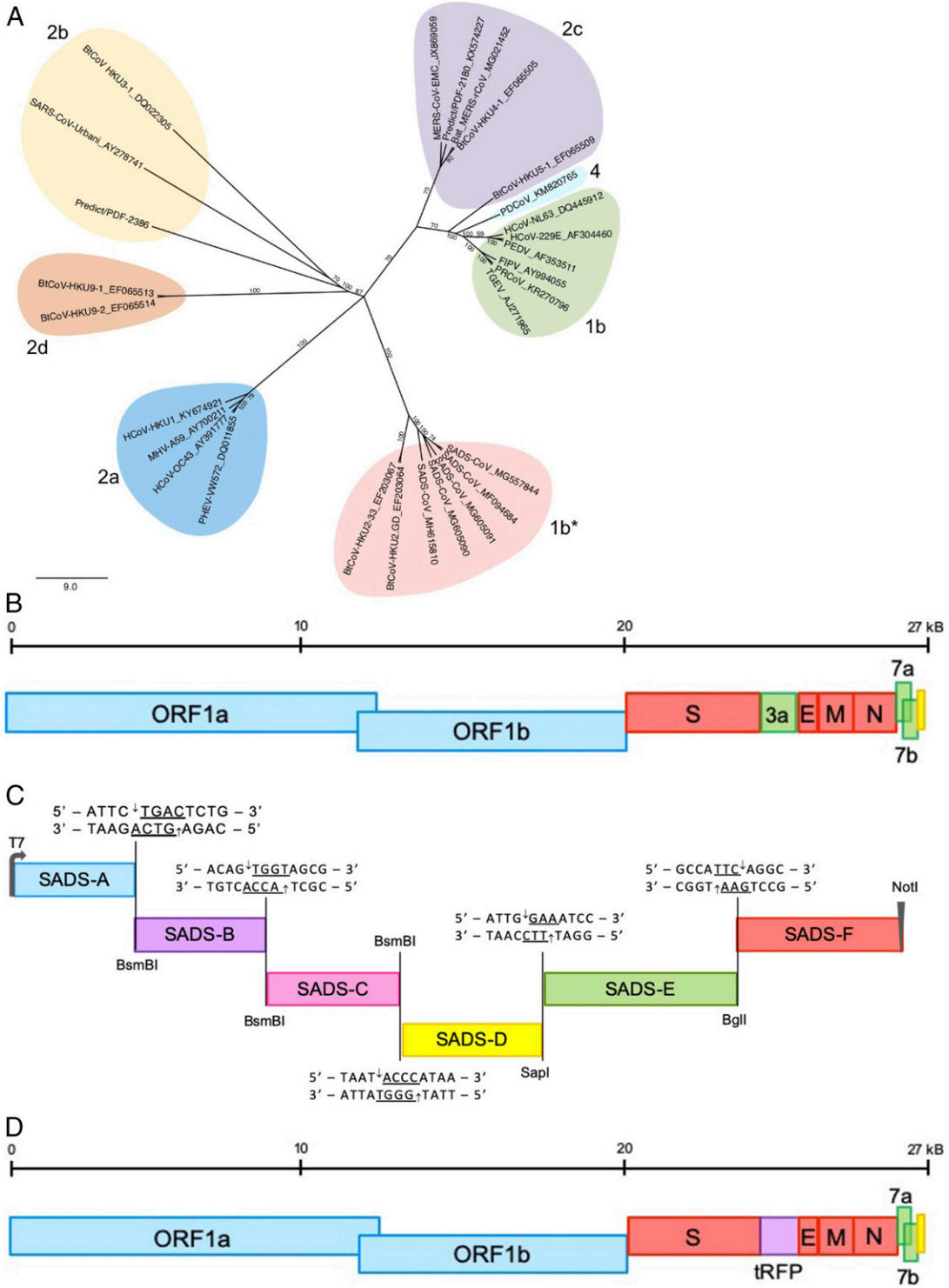

Fig. 1. Spike phylogeny of representative coronaviruses and organization of the SADS-CoV wild-type and RFP infectious clones. (*A*) The S protein sequences of selected coronaviruses were aligned and phylogenetically compared. Coronavirus genera are grouped by classic subgroup designations (1b, 2a–d, 4). Sequences designated as 1b* (including SADS-CoV and related viruses) group with 1b viruses in proteins other than S. Sequences were aligned using free end gaps with the Blosum62 cost matrix in Geneious Prime. The tree was constructed using the neighbor-joining method based on the multiple sequence alignment, also in Geneious Prime. Numbers following the underscores in each sequence correspond to the GenBank accession number. The radial phylogram was rendered for publication using Adobe Illustrator CC 2019. (*B*) The general arrangement of the SADS-CoV genome. Blue represents nonstructural proteins ORF1a and ORF1b. Red represents structural proteins spike, envelope, membrane, and nucleocapsid. Green represents accessory proteins 3a, 7a, and 7b. Yellow represents the untranslated region. (*C*) The full-length infectious clone was divided into six contiguous cDNAs flanked by either BsmBI (SADS-CoV A–C), SapI (SADS-CoV D), BglI (SADS-CoV E–F) to allow for efficient assembly of the full-length SADS cDNA. BsmBI and SapI are not present in the viral genome sequence but are introduced externally in the fragment plasmid sequence. SADS-CoV A (nucleotides 1 to 4,496), SADS-CoV B (nucleotides 4,497 to 8,996), SADS-CoV C (nucleotides 8,997 to 13,496), SADS-CoV D (nucleotides 13,497 to 17,997), SADS-CoV E (nucleotides 17,998 to 22,892), and SADS-CoV F (nucleotides 22,893 to end). (*D*) General organization of SADS-CoV tRFP depicting the insertion of tRFP in place of NS3a.

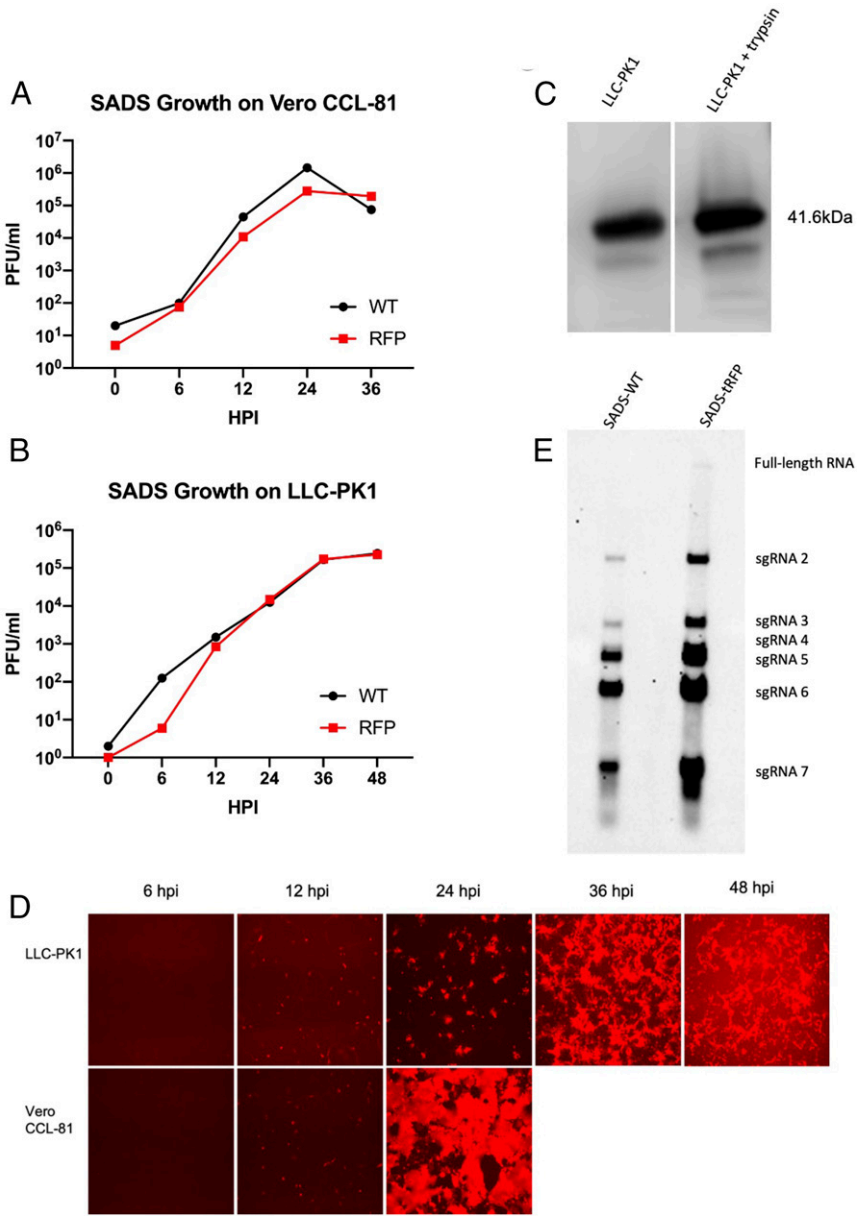

Fig. 2. Growth of wild-type and tRFP SADS-CoV. Growth of SADS-CoV wild-type and tRFP infectious clones compared in Vero CCL-81 (*A*) and LLC-PK1 (*B*) cultures. All supernatants were titered on Vero CCL-81 cells. Viral titers grew to mid-10^5 to 10^7 PFU/mL in these cell types, with the highest titers seen in Vero CCL-81 cells. (*C*) Cultures of LLC-PK1 cells infected with SADS-CoV and protein lysates were run on Western blots with and without trypsin for comparison. Cell lysates were probed with antinucleocapsid antibodies from sera of mice immunized with VRP. N proteins (41.6 kDa) were present among both conditions. (*D*) tRFP expression of Vero CCL-81 and LLC-PK1 cultures is shown at 10× magnification. By 36 h, cytopathic effect in Vero CCL-81 cultures was complete. (*E*) Northern blot analysis of wild-type SADS and SADS tRFP for leader containing transcripts of known ORFs.

growth in HNE and HAE cultures approached 10^5 PFU/mL (Fig. 4 *B* and *C* and *SI Appendix*, Fig. S4*A*). Importantly, SADS-CoV also replicated efficiently in primary human intestinal cells (Fig. 4*D* and *SI Appendix*, Fig. S4*B*), replicating to titers of 10^5 PFU/mL over 96 hpi (Fig. 4*F*). As seen with other coronaviruses, such as SARS-CoV-2 (34), SADS-CoV infection in primary cells is donor dependent with replication efficiency varying between patients. SADS-CoV replication was validated by RT-PCR evidence of N gene mRNA transcripts and for N gene protein expression by Western blot in several primary cell lines (Figs. 2*C*, 3*C*, and 4 *E* and *G* and *SI Appendix*, Fig. S3). These data demonstrate that the host range of SADS-CoV is very broad, providing potential opportunities for spillover from bats to swine or to other economically important intermediate or companion hosts, including humans (35–37).

For many virus families, herd immunity to contemporary human viruses can cross-neutralize and minimize the potential for zoonotic virus cross-species transmission and emergence in nature (38–43). To provide some guidance for potential future outbreak control, we next tested whether human convalescent sera to related group 1 coronavirus HCoV NL63 could cross-neutralize SADS-CoV tRFP. Treatment with several human coronavirus sera provided little if any cross-neutralization of SADS-CoV in Huh7.5 cells. Under identical conditions, the sera effectively neutralized another group 1b CoV, HCoV NL63 (Fig. 5 *A* and *B*). Additionally, we evaluated the capacity of a broad-spectrum coronavirus nucleoside antiviral, remdesivir, to inhibit rSADS-CoV tRFP replication in Huh7.5

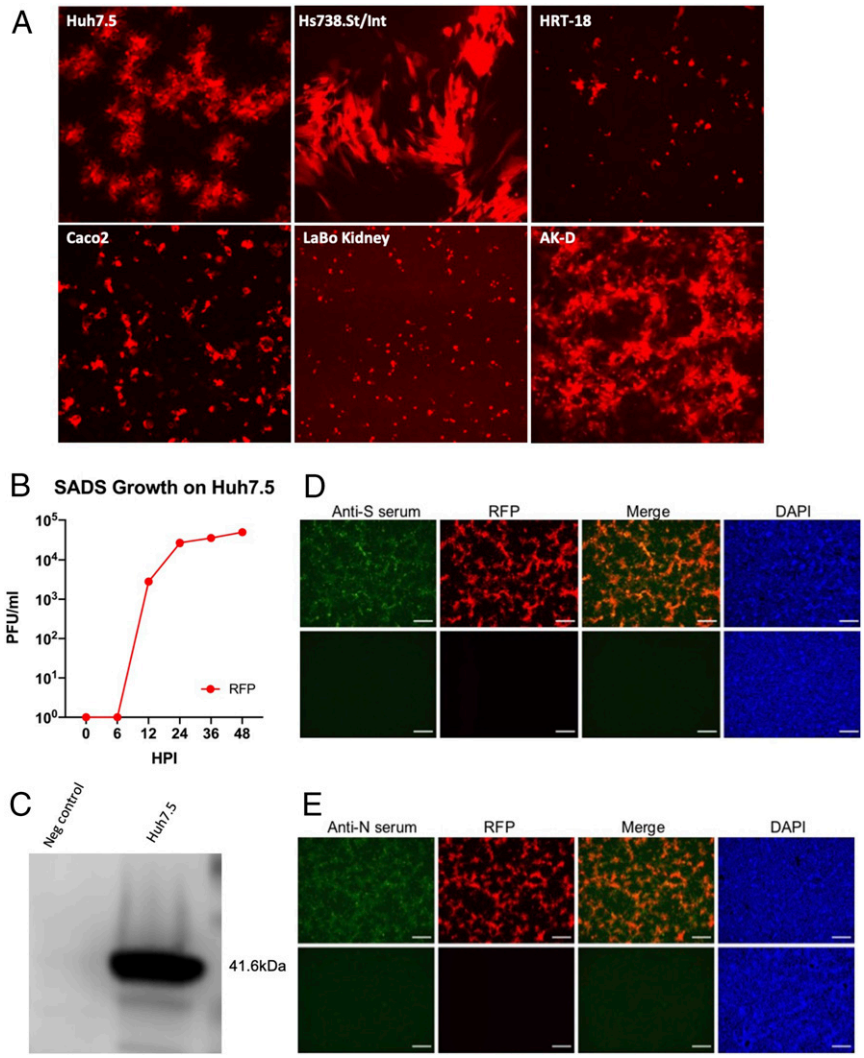

Fig. 3. Host range of SADS tRFP. (*A*) Cultures of human Huh7.5 liver, human Hs738.St/Int stomach-intestine, human colo-rectal HRT-18 tumor, Caco2, LaBo kidney, and feline AK-D lung cells were infected with SADS tRFP. All cell types, with the exception of Caco2 and Huh7.5 cells, were cultured in the presence of trypsin to enhance virus infectivity. Cultures were visualized at 48 hpi for fluorescence at 10× magnification. (*B*) Growth of SADS-tRFP in Huh 7.5 cells. (*C*) Cultures of Huh7.5 cells were infected with SADS-CoV and lysed for analysis by Western blot. N protein has a molecular mass of ∼41.6 kDa. Immunofluorescent images of Vero CCL-81 cells infected with mock or SADS-CoV tRFP virus and stained with mouse anti-N (*D*) or anti-S (*E*) sera. Cultures were fixed at 24 hpi and viral proteins were visualized by immunostaining with antisera isolated from VRP S or VRP N vaccinated mice. Scale bars represent 100 μm.

cells. In a concentration-dependent manner, remdesivir efficiently inhibited SADS-CoV replication, as evidenced by reduced tRFP expression and reduced virus titers after treatment (Fig. 5*C* and *SI Appendix*, Fig. S5).

SADS-CoV Receptor Interactions. During SARS-CoV and HCoV NL63 infections, the S glycoprotein binds the human angiotensin converting enzyme 2 (ACE-2) receptor to direct entry into the cell (44). During MERS-CoV infection, the virus binds human dipeptidyl peptidase 4 (DPP4) as a receptor to mediate infection of human cells (45), while TGEV and some related group I coronaviruses use aminopeptidase N (APN or CD13) (46). Consequently, we treated Huh7.5 cells with polyclonal antibodies against human DPP4 or human APN (CD13) under conditions that block MERS and HCoV 229E infection (47, 48). After 1 h, the cultures were inoculated with SADS-CoV tRFP. Additionally, DBT cells expressing human ACE-2 were tested for their ability to support SADS-CoV tRFP replication. Using tRFP as a readout, we found no evidence of altered viral infectivity and replication in Huh7.5 in the presence of high concentrations of either antireceptor antibody, and SADS-CoV did not replicate in DBT–ACE-2 cells (Fig. 6). These data suggest that SADS-CoV does not use any of these known coronavirus receptors for docking and entry into human cells.

In Vivo Mouse Model Availability. Previous studies have reported that SADS-CoV replicates to low levels in wild-type laboratory mice (29). To enhance this model, identify host functions that may modulate SADS-CoV infection severity, and evaluate drug performance, we inoculated type I/II IFNR-immunodeficient mice with 1×10^5 PFU of SADS-CoV by either intraperitoneal injection or oral gavage. Upon using qRT-PCR to detect genome-length mRNA and the most abundant single-guide RNA 6, we noted little, if any, evidence of reproducible or robust virus replication in the liver, spleen, or various sections of the intestine at day 2 (*SI Appendix*, Fig. S6*A*). In fact, only 1 of 12 animals had evidence of low-level virus gene expression in multiple tissues. While a few other samples contained sporadic, low-level SADS mRNA, the positive tissues were not consistent across organs or mice and indicate a nonproductive infection that fails to replicate, at best. In wild-type BALB/c mice, we also saw little, if any, evidence of measurable

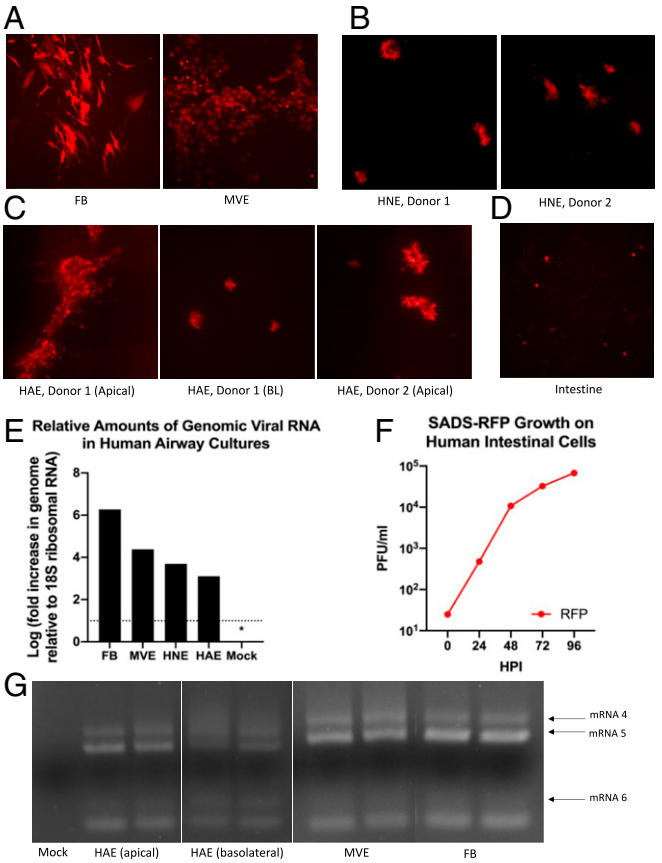

Fig. 4. Susceptibility of human primary cells to SADS-CoV. (*A*) Human FB and MVE cells ($n = 3$, each) were infected with SADS-CoV. By 72 hpi, abundant infection of both FB and MVE cells by SADS-RFP was observed. (*B*) HNE cells from two donors ($n = 3$) were infected with SADS-RFP, demonstrating comparable RFP infection by 72 hpi. (*C*) HAE cells were infected both basolaterally and/or apically (donor 1) or apically (donor 2) and observed for 96 h or 72 h, respectively. (*D*) Human primary intestinal cultures ($n = 2$) were infected with SADS-RFP and were observed for 96 hpi. All fluorescent images were taken at 10× magnification. (*E*) qRT-PCR of genomic mRNA from primary human lung cells infected with SADS-CoV. Cultures from various codes were averaged to determine amounts of genomic viral RNA. No detectable viral signal was observed in mock-infected cultures from each cell type, as indicated by the * representing half the limit of detection. Levels of viral genome were determined in infected and mock cultures, relative to 18S ribosomal RNA. (*F*) Virus samples were taken from primary intestinal cells every 24 hpi, and growth determined by plaque assay. (*G*) RT-PCR of leader containing transcripts, run in duplicate, indicate presence of SADS-CoV mRNA in MVE, FB, and HAE cells.

replication in vivo at day 2 postinfection (*SI Appendix*, Fig. S6*B*). While IFNR-immunodeficient mice have been shown to enhance the replication of other coronaviruses in vivo (49, 50), this defect had no substantial positive effect on SADS-CoV growth under our treatment conditions. These data are consistent with the interpretation that SADS-CoV does not replicate efficiently in *Mus musculus domesticus* mice and that most, if not all, of the positive signal is arising from abortive infections or input virus. Thus, our data argue that standard laboratory mouse models are clearly insufficient to provide opportunities for studying viral pathological mechanisms or in evaluating the performance of antivirals and vaccines.

Discussion

Coronaviruses, as well as other zoonotic virus families—such as orthomyxoviruses, paramyxoviruses, enteroviruses, and filoviruses—represent high-threat pathogens to One Health and the global economy (51, 52). The recent emergence of novel human and animal coronaviruses dictates the need for new strategies to identify higher-risk strains that may seed future disease outbreaks. Most emerging human and animal coronaviruses, including the recently emerged SARS-CoV-2, probably originated from bats (3, 27, 53–55) and have the capacity to evolve and spread rapidly across the globe (56–58). Contemporary human and swine strains have become fully adapted to their hosts, although some retain the capacity to replicate in bat cells (27). Using large numbers of bat CoV polymerase sequences from multiple bat species, recent

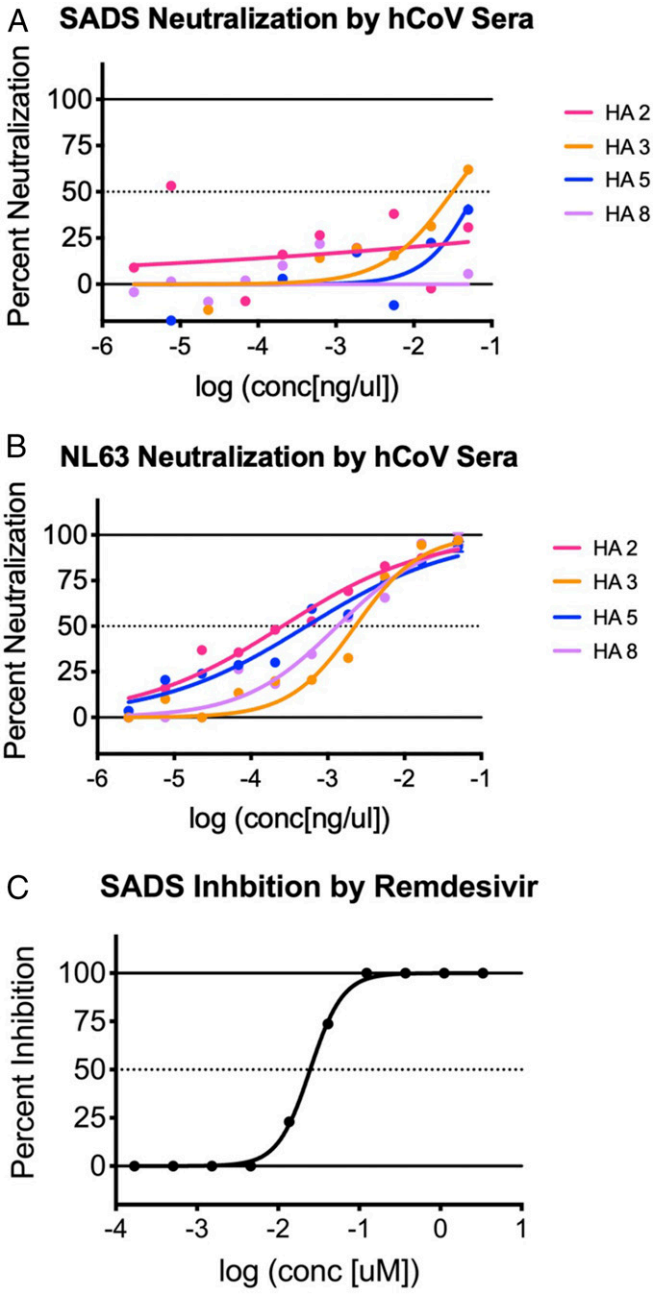

Fig. 5. Neutralization and inhibition of SADS-CoV. Neutralization assays were run using human CoV donor sera against SADS-CoV (*A*) and HCoV NL63 (*B*), a known human coronavirus. Very little, if any, neutralization of SADS was seen compared to neutralization of HCoV NL63. (*C*) Remdesivir, a known antiviral, inhibited SADS-CoV virus growth, indicating a potential therapeutic for possible human infection.

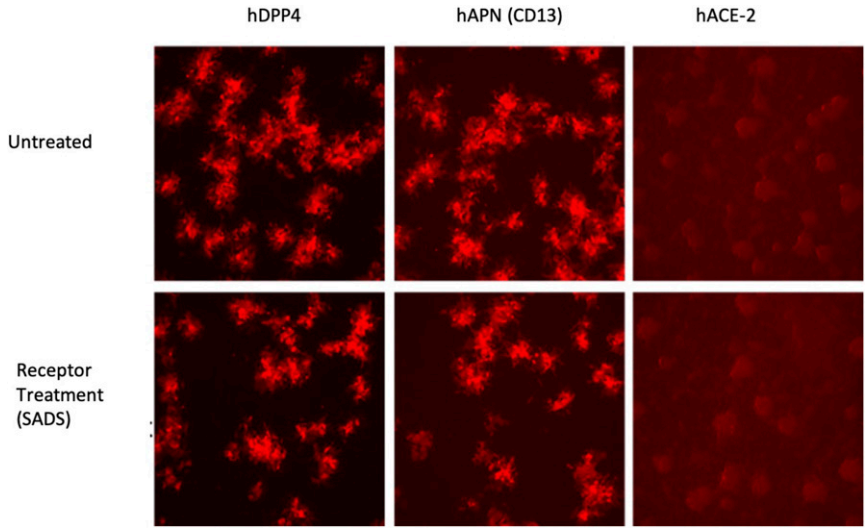

Fig. 6. Potential receptors for SADS-CoV. Huh7.5 cells were treated with antibody against DPP4 or CD13 and then infected with SADS-CoV GFP. When compared to the untreated cultures, all cells and antibody treatment conditions did not block SADS-CoV entry or replication, suggesting that SADS-CoV is not using a known coronavirus entry receptor. Control DBT and DBT cells expressing hACE-2 were also infected and shown to be not permissive for SARS-CoV 2 GFP growth. All fluorescent images were taken at 10× magnification.

studies argue that the α-CoVs have a much higher likelihood to switch hosts within their natural bat reservoirs than the β-CoVs, implying high spillover risk to other mammalian species (59). In support, recent findings indicate that SADS-CoV swine outbreaks have likely originated from multiple spillover events from exotic bats in China, and may readily cycle between these species (10). In this report, we demonstrate human susceptibility potential by demonstrating efficient SADS-CoV infectivity and growth in primary human cells, derived from both the lung and intestine (33). Moreover, efficient SADS-CoV replication in the primary intestinal cells also support an earlier hypothesis that some emerging bat coronaviruses may initially replicate efficiently in the human alimentary track and stroma, before evolving efficient replication phenotypes in the lung (25).

With increased access to global travel and frequent human-to-human interaction, it is crucial to develop and utilize strategies to understand the risk potential of emerging viruses to One Health globally. In this study, we used metagenomics, bioinformatics, synthetic genome design, and reverse genetics to recover recombinant wild-type and derivative SADS-CoVs from in silico sequence databases. Using this model, we studied virus genome organization and expression patterns in infected cells and evaluated the capacity of human serum and small-molecule inhibitors to impede SADS-CoV growth in vivo. The molecular clone and work described herein expands upon a recently published swine enteric alphacoronavirus molecular clone (60) by: 1) Generating mutants that demonstrated a nonessential role for ORF3 is virus growth in vitro; 2) the development of indicator viruses, which revealed new insights into the broad host range; 3) studying cross-group 1b neutralization; and 4) identifying SADS-CoV susceptibility to a broad-spectrum nucleoside chain terminator, remdesivir, which has been used to treat lethal Ebola infections with some success (61). Additionally, remdesivir is effective at reducing SARS-CoV-2 infection and has been cleared for emergency use in treating COVID-19 patients (62, 63). Previous studies in our laboratory and others have shown that remdesivir was broadly active against alpha-, beta-, and gammacoronaviruses both in vitro and in vivo (64–66). As SADS-CoV is highly susceptible to remdesivir treatment in vitro, these findings support its potential use in the event of possible future SADS-CoV or related HKU2 disease outbreaks. In mouse models of human disease, remdesivir is very effective at treating lethal SARS-CoV2 infection (67) and MERS-CoV infection than combination lopinavir, ritonavir, and IFN-β (68). In contrast to other reports, SADS-CoV replication in wild-type mice was minimal at best. We noted little evidence of significant or reproducible replication across animals or tissues at day 2, indicating the need for a proper small-animal model for use in in vivo antiviral or vaccine testing (*SI Appendix*, Fig. S5). Our inability to enhance SADS-CoV growth in immunodeficient IFNR$^{-/-}$ mice provide further evidence that the mouse is not a suitable model for SADS-CoV pathogenesis, vaccine, or therapeutic studies, revealing a vulnerability in global preparedness.

The emergence of PEDV in the United States and China was associated with devastating economic losses in the swine industry (69, 70). SADS-CoV is closely related to HKU2 alphacoronavirus of bats, which was first identified in Hong Kong and Guangdong Province, China, in 2007 (15). Although SADS-CoV S glycoprotein variation is limited across outbreaks, HKU2-like strains are widely dispersed throughout Europe, Southeast Asia, and elsewhere and encode diverse S glycoprotein genes that vary by as much as 15% (Fig. 1*A*) (10, 71). Although speculative, one or more of these diverse HKU2-related strains may also encode broad host range or transmission potentials, like SADS-CoV, enhancing the potential for animal and human outbreaks. The development of a stable molecular clone that can be used to recover wild-type and derivative recombinant viruses encoding different HKU2 S glycoprotein genes provides a robust platform to address this important One Health concern. Importantly, SADS-CoV has caused severe disease outbreaks in herds vaccinated with attenuated PEDV, illustrating the inability of existing swine PEDV vaccines to elicit protective immune responses against this emerging pathogen (17). The major component of protective immunity for coronaviruses usually targets the S glycoprotein and, to a lesser extent, the N protein (72). Given the extensive amino acid differences between contemporary human group 1b CoV and SADS-CoV S genes, it is not surprising that human sera efficiently neutralized hCoV NL63, but not SADS-CoV (Fig. 5 *A* and *B*). Taking these data together, we find that the inability for PEDV vaccines and human polyclonal sera to protect against the SADS-CoV suggest that little, if any, cross-coronavirus herd immunity would exist to control the spread of this new pathogen, especially in swine. As previous studies have

demonstrated that alphavirus VRP vaccines encoding the N and S proteins can provide protection against lethal SARS-CoV and MERS-CoV infection and protect swine from PEDV infection (73), the SADS VRP N and S VRP vaccines developed herein may provide for similar opportunities for controlling SADS-CoV, and perhaps other group 1b swine coronavirus infections (74).

The coronavirus S glycoprotein is usually cleaved into distinct S1 and S2 polyproteins that include well-defined domains, including the S1 N-terminal domain (NTD) and C-terminal domain (CTD) (75). In some coronaviruses, the NTD contains folds that bind sugar residues, while the CTD encodes the receptor-binding domain, which engages various receptors, such as ACE-2, DPP4, CECAM1, and CD13 (75). SADS-CoV targeted a variety of host cell types from multiple species, including those characterized as of both human and nonhuman origin. The surprisingly broad host range of SADS-CoV does not appear to be driven by ACE-2, DPP4, or CD13 receptor usage, as antibodies targeting these receptors do not inhibit virus replication in human cells and overexpression of the human ACE-2 receptor also did not promote replication in mouse cells. As protease treatment enhances SADS-CoV host range, the data are also consistent with extensive literature that argues that protease availability is also a key regulator of coronavirus cross-species transmission (76–78). rSADS-CoV tRFP replication in various immortalized human cells, including liver, stomach, intestinal, and rectal tumor cells (Fig. 3*A*). However, a group 1 CoV camel coronavirus that was closely related to HCoV 229E also showed efficient replication in human tumor cell lines, but not in primary human lung airway cells, demonstrating the critical importance of evaluating zoonotic virus species specificity in primary cells (33). In contrast and in the absence of exogenous proteases, SADS-CoV replicated efficiently in primary human endothelial cells, primary lung fibroblasts cells, but growth in primary human airway and nasal epithelial cells. These cells play critical roles in maintaining lung architecture, compartmentalization, and airway function (79). Lung fibroblasts also play a central role in the homeostasis of the extracellular matrix and are effector cells during injury repair, while the microvascular endothelium regulates vascular homeostasis, as vascular leak can result in inefficient gas exchange in the lungs (80). In parallel, we showed efficient growth in primary human intestinal cells, including high virus titers after infection. Together, these data forge a compelling argument regarding potential human susceptibility to SADS-CoV infections. Future studies must focus on identifying the entry and species-specificity mechanisms that regulate SADS-CoV cross-species transmission and pathogenesis, as well as the potential array of evolutionary pathways that could evolve to promote efficient replication in different human cells and tissues.

The emergence of the group 2b SARS-CoV-2 in Wuhan, China SADS-CoV demonstrated the predictive utility of using primary human lung cells, receptor interaction, and antigenic studies to predict the preepidemic potential of novel zoonotic viruses, and then use this recombinantly derived collection of viruses to identify readily available drugs for compassionate use (6–8, 66, 68). SADS-CoV also has a broad host range and replicates efficiently in primary human lung and intestinal cells. Due to the variability in infection efficiency seen between various donors of human primary cells, it is likely that in the case of a spillover, we would see a range of SADS-CoV severity in human patients. Swine are known amplifying hosts for several human pathogens, providing an infrastructure for the possibility of future emergence events. To date, there is no evidence of virus replication in humans (10). However, the ability of SADS-CoV to replicate in human primary cells indicates the potential for spillover of SADS-CoV into humans. With the 2019 reemergence of this virus in the swine population in China (81), continued surveillance of swine is critical. Additionally, individuals in the swine industry should be regularly evaluated for evidence of infection in order to reduce the potential of outbreaks. Consistent with the phylogenetic distance in the S glycoproteins (Fig. 1*A*), little, if any, significant levels of cross-neutralizing human or swine herd immunity appear to exist between the contemporary alphacoronavirus tested and the SADS-CoV. While recognizing an unexplored potential for T cell contributions and given this collection of phenotypes, we suggest the need for continued One Health surveillance (82, 83), screening of swine workers in outbreak settings, BSL3 containment and that the development and testing of candidate vaccines and drugs should be prioritized to protect the health of human populations as well as economically important domesticated livestock.

Materials and Methods

Virus and Cells. The recombinant SADS-CoV and its RFP-expressing derivative (SADS-CoV tRFP) were propagated in Vero CCL-81 and LLC-PK1 cells. All cells were maintained prior to infection in complete DMEM media supplemented with 10% serum, nonessential amino acids, sodium pyruvate, and 1% antibiotic. To generate virus stocks, cells were washed twice with PBS and cultured in serum-free DMEM-H media supplemented with 8% tryptose phosphate broth and 2.5 to 10 μg/mL trypsin and grown at 37 °C in a humidified CO_2 incubator. Samples were then titered by plaque assay on Vero CCL-81 cells. To enhance viral growth and spread, 10 μg/mL trypsin was added to the overlay for plaque assay. Growth curves were performed in Huh7.5 and LLC-PK1 cells, and supernatants were titered on Vero CCL-81 cells as previously described (84, 85). Huh7.5 cells did not require additional trypsin for viral growth and spread, although it is likely that the inoculum used to perform the growth curves contained minimal levels of residual trypsin. For growth curves of SADS-CoV tRFP, fluorescent foci were counted to determine titer. Primary human airway epithelial cells, lung fibroblast, and lung microvascular endothelial cells prepared as described previously (86) were purchased from the Marsico Lung Institute, Tissue Procurement and Cell Culture Core, University of North Carolina at Chapel Hill, and used to evaluate SADS-CoV growth using previously described methods (84, 85). The cells obtained from human lungs were approved by the University of North Carolina at Chapel Hill Biomedical Institutional Review Board (protocol #03-1396). Two-dimensional primary human intestinal cells were derived from human ileal crypts that form a continuous polarized epithelium with proliferative and nonproliferative zones (87). All primary cells (lung and intestinal) were infected with SADS-CoV tRFP diluted at 1:10 in PBS. Inoculated cultures were incubated at 37 °C in a humidified CO_2 incubator for 2 h before washing with PBS. Viral titers were determined using apical washes of airway ALI cultures, or apical media of intestinal cultures at appropriate time points. All recombinant SADS-CoVs were maintained in a BSL3 laboratory to enhance biosafety and all waste material was disinfected and autoclaved prior to removal from the facility. All personnel were equipped with fully protective Tyvek suits, double gloves, and a powered air-purifying respirator, as previously described by our group (8).

Systematic Assembly of a Full-Length SADS-CoV cDNA. The SADS-CoV clone was designed using the previously published sequence (10). Six contiguous cDNAs (A–F) flanked by unique restriction endonuclease sites (BsmBI/SapI/BglI) were purchased from BioBasic (Fig. 1). Breakpoints were designed to maximize the stability of cloned fragments in bacteria as previously described by our group (21–24). The fragments were digested, separated through 0.8% agarose gels, visualized, excised, and purified using a QIAquick Gel Extraction Kit. The SADS-CoV cDNAs were ligated overnight at 4 °C, phenol/chloroform extracted, and precipitated. Full-length T7 RNA transcripts were generated in vitro as described by the manufacturer with modifications (21). RNA transcripts (wild-type or tRFP) were added to a Vero CCL-81 cell suspension (8×10^6) in an electroporation cuvette, and four electrical pulses of 450 V at 50 μF were distributed with a Gene Pulser II electroporator (Bio-Rad). As previously published, N gene transcripts were included during electroporation due to the increased infectivity of coronavirus transcripts when incorporated (20, 21). Transfected cells were allowed to recover at room temperature before incubating at 37 °C for 4 d in a 75-cm^2 tissue culture flask. Viral progeny were passaged once in either Vero CCL-81 or LLC-PK1 cells for 2 to 4 d and used to generate a virus stock for future use (GenBank, accession no. MT039231).

Recombinant SADS-CoV tRFP Expression Construct. To generate a SADS-CoV tRFP recombinant virus, the nonstructural ORF, NS3a, was replaced with tRFP via generation of three PCR amplicons and ligation into the SADS F fragment. One PCR amplicon was generated using primers SADS tRFP #1+ (5′-gtg cattgttgctaaggacgg-3′) and SADS tRFP #2 rev (5′-nnnnnngctcttcttggacgtggac cttttcaatctc-3′). A second PCR amplicon was generated using primers SADS

tRFP #3+ (5′-nnnnnngctcttctccaataatggtgagcaagggcgaggag-3′) and SADS tRFP #4 rev (5′-nnnnnngctcttcattacttgtacagctcgtccatg-3′). A third PCR amplicon was generated using primers SADS tRFP #5+ (5′-nnnnnngctcttcgtaatactaacacacctt ttgttggtatc-3′) and SADS tRFP #6 rev (5′-ggcgcaaagagtgacaatgg-3′). The three amplicons were digested with SapI, as indicated in the primer sequences above, and ligated. The ligation product was then digested with Bpu10I and EciI prior to insertion into the SADS F plasmid. Recovery of recombinant viruses encoding tRFP are as described previously (GenBank, accession no. MT039232) (20, 21).

VRP Expressing SADS N and S Genes. The SADS N and S genes were cloned separately into pVR21 3526 to generate VRPs, as previously described (28, 88). Briefly, pVR21 is an expression vector carrying the VEE genome in which the VEE structural genes are replaced by the SADS N or S gene following the 26S promoter. The SADS N and S gene, with the deletion of 7 amino acids from the C terminus, was PCR-amplified off the full SADS cDNA before insertion into the pVR21 backbone. The SADS-pVR21 construct, a plasmid containing the VEE 3526 envelope glycoproteins, and a plasmid containing the VEE capsid protein were used to generate T7 RNA transcripts. The RNA transcripts were then electroporated into BHK cells. VRP were harvested 48 h later and purified via high-speed ultracentrifugation. Groups of 5- to 7-wk-old BALB/c mice (Jackson Labs) were then inoculated via footpad injection with VRP expressing the SADS N protein. Mice were boosted at 21 d, killed at 14 d postboost, and serum was collected for antibody against the N protein.

Western Blot Analysis. To produce protein lysates for analysis by Western blot, infected cells were washed with 1× PBS and lysed in buffer containing 20 mM Tris·HCl (pH 7.6), 150 mM NaCl, 0.5% deoxycholine, 1% nonidet P-40, 0.1% SDS. After initial lysis and removal of nuclei, supernatants were added to an equal volume of 10 mM EDTA and 0.9% SDS. Following lysis, samples were incubated for 15 min at room temperature prior to use in Western blot. Proteins were separated using a 7.5% polyacrylamide gel. For each sample, protein lysate was mixed with 4× loading dye and heated to 95 °C for 10 min. Samples were loaded into the gel and separated by electrophoresis in 1× running buffer at 110 V for 5 min, followed by 90 V for 65 min. Proteins were transferred onto an Immuno-Blot polyvinylidene difluoride (PVDF) membrane at 115 mA for 30 min using 1× dry transfer buffer. The membranes were blocked in 1× PBS–Tween 20 (PBST)–5% milk at 4 °C overnight with shaking. Membranes were then treated with primary antibody using mouse anti-SADS nucleocapsid sera (1:250) and incubated at 37 °C for 2 h with shaking. Membranes were washed three times with 1× PBST before treatment with secondary antibody. Secondary antibody of goat anti-mouse IgG HRP (1:5,000) and were incubated at room temperature for 1 h with shaking. Membranes were washed six times with 1× PBST (5 min per wash) and developed using LI-COR WesternSure PREMIUM Chemiluminescent Substrate. Membranes were incubated at room temperature for 5 min before imaging was performed using the LI-COR C-DiGit blot scanner.

Northern Blot Analysis. Total RNA was extracted from icSADS or icSADS-tRFP infected cells approximately 20 hpi using TRIzol Reagent. Messenger [poly(A)] RNA was isolated from the total RNA using an Oligotex mRNA Mini Kit. Messenger RNA (0.6 to 0.7 μg) was separated on an agarose gel and transferred to BrightStar-Plus membrane using a NorthernMax-Gly Kit. Blots were hybridized with a biotin-labeled oligomer (5′-BiodT/CTTTGATTACTCCACCA-CACCAGACA/BiodT-3′), then detected using a Chemiluminescent Nucleic Acid Detection Module.

RT-PCR of Leader Containing Transcripts. RNA, isolated using TRIzol Reagent, was reverse transcribed using a SuperScript II kit and random primers. PCR was performed using a SADS leader primer (5′-GACTTTCCAGTCTACTCTTCTC-3′) and a reverse primer in the N gene (5′-CGAGACTGTGAACGTGAAGC-3′).

In Vivo Infection of BALB/C and IFNR Mice. Ten-week-old BALB/c or IFN type I/II knockout mice (IFNR) were infected with 1×10^5 PFU of SADS-CoV. IFNR mice were infected either intraperitoneally or by oral gavage, and BALB/c mice were infected intranasally or by oral gavage. Mice infected by all inoculation routes were given 1×10^5 SADS-CoV per route. Mice were weighed daily, and samples were harvested at 2 d postinfection, including the liver, spleen, and intestines. Intestinal samples were harvested by section including duodenum, jejunum, ileum, and colon. RNA was extracted from each tissue sample and qRT-PCR was run to determine the amount of viral RNA present in each mouse and tissue. These experiments were approved by University of North Carolina's Insitutional Animal Care and Use Committee (IACUC).

Neutralization Assays with hCoV Sera. Neutralization assays were performed using known hCoV sera against SADS-CoV tRFP and NL63 GFP, using methods previously described (89). NL63 GFP was used as a hCoV expected to be neutralized by human donor sera. SADS-CoV tRFP and NL63 GFP diluted to 10^5 PFU were incubated with sera from four donors at 1:2 serial dilutions for 1 h at 37 °C. All dilutions were performed in serum-free media containing 1% antibiotic. Poly-L-lysine treated 96-well plates seeded with Huh7.5 cells were infected with each condition of virus and sera, as well as with PBS and sera-free virus as controls, for 1 h at 37 °C for SADS-CoV tRFP and 32 °C for NL63 GFP. Following infection, virus and sera was removed and cells were washed twice with 1× PBS before overlaid with serum-free media. Cells were imaged for fluorescence and percent neutralization was calculated using the area of fluorescence.

Inhibition of SADS-CoV by Remdesivir. Poly-L-lysine–treated 96-well plates seeded with Huh7.5 cells were infected with SADS-CoV tRFP diluted to 2×10^5 PFU in the presence of a dose–response of remdesivir or DMSO for 1 h at 37 °C. Following infection, virus was removed, and cells were overlaid with serum-free media containing DMSO or the dose–response of remdesivir. Cells treated with DMSO, but not virus, were included as a negative control to serve as the 100% inhibition marker. Cells were imaged for fluorescence and percent inhibition was calculated using the area of fluorescence.

Biosafety. Due to the potential for human susceptibility to SADS-CoV infection, we recommend that work with this virus continue to be done under BSL3 conditions.

Data Availability. The sequences of recombinant SADS-CoV viruses have been deposited in GenBank under (accession nos: MT039231 for rSADS-CoV wild-type (90) and MT039232 for rSADS-CoV tRFP (91). All other study data are included in the main text and *SI Appendix*.

ACKNOWLEDGMENTS. Provision of primary human lung cells by Dr. Randell was supported by grants from the Cystic Fibrosis Foundation (BOUCHE19R0) and NIH (DK065988). We thank Dr. Camille Ehre for providing the primary human intestinal cells for this study. This project was supported by the North Carolina Policy Collaboratory at the University of North Carolina at Chapel Hill with funding from the North Carolina Coronavirus Relief Fund established and appropriated by the North Carolina General Assembly. This work was also supported by NIH Grants AI089728, AI142759, AI132178, and AI151797 (to R.S.B.). The content is solely the responsibility of the authors and does not necessarily represent the official views of the NIH.

1. J. S. Mackenzie, M. Jeggo, The One Health approach—Why is it so important? *Trop. Med. Infect. Dis.* **4**, 88 (2019).
2. Q. Wang, A. N. Vlasova, S. P. Kenney, L. J. Saif, Emerging and re-emerging coronaviruses in pigs. *Curr. Opin. Virol.* **34**, 39–49 (2019).
3. V. M. Corman, D. Muth, D. Niemeyer, C. Drosten, Hosts and sources of endemic human coronaviruses. *Adv. Virus Res.* **100**, 163–188 (2018).
4. WHO, Middle East respiratory syndrome coronavirus (MERS-CoV)—Update, https://www.who.int/csr/don/2014_07_23_mers/en/. Accessed 7 October 2019.
5. WHO, Summary of probable SARS cases with onset of illness from 1 November 2002 to 31 July 2003, https://www.who.int/csr/sars/country/table2004_04_21/en/. Accessed 7 October 2019.
6. X.-Y. Ge *et al.*, Isolation and characterization of a bat SARS-like coronavirus that uses the ACE2 receptor. *Nature* **503**, 535–538 (2013).
7. V. D. Menachery *et al.*, A SARS-like cluster of circulating bat coronaviruses shows potential for human emergence. *Nat. Med.* **21**, 1508–1513 (2015).
8. V. D. Menachery *et al.*, SARS-like WIV1-CoV poised for human emergence. *Proc. Natl. Acad. Sci. U.S.A.* **113**, 3048–3053 (2016).
9. WHO, Novel coronavirus—China, https://www.who.int/csr/don/12-january-2020-novel-coronavirus-china/en/. Accessed 7 February 2020.
10. P. Zhou *et al.*, Fatal swine acute diarrhoea syndrome caused by an HKU2-related coronavirus of bat origin. *Nature* **556**, 255–258 (2018).
11. K. Jung, H. Hu, L. J. Saif, Porcine deltacoronavirus infection: Etiology, cell culture for virus isolation and propagation, molecular epidemiology and pathogenesis. *Virus Res.* **226**, 50–59 (2016).
12. J. C. Mora-Díaz, P. E. Piñeyro, E. Houston, J. Zimmerman, L. G. Giménez-Lirola, Porcine hemagglutinating encephalomyelitis virus: A review. *Front. Vet. Sci.* **6**, 53 (2019).
13. L. J. Saif, J. L. van Cott, T. A. Brim, Immunity to transmissible gastroenteritis virus and porcine respiratory coronavirus infections in swine. *Vet. Immunol. Immunopathol.* **43**, 89–97 (1994).
14. P. C. Woo *et al.*, Coronavirus HKU15 in respiratory tract of pigs and first discovery of coronavirus quasispecies in 5′-untranslated region. *Emerg. Microbes Infect.* **6**, e53 (2017).
15. L. Gong *et al.*, A new bat-HKU2-like coronavirus in swine, China, 2017. *Emerg. Infect. Dis.* **23**, 1607–1609 (2017).

16. X. Huang *et al*., Human coronavirus HKU1 spike protein uses O-acetylated sialic acid as an attachment receptor determinant and employs hemagglutinin-esterase protein as a receptor-destroying enzyme. *J. Virol.* **89**, 7202–7213 (2015).
17. L. Zhou, The re-emerging of SADS-CoV infection in pig herds in southern China. *Transbound. Emerg. Dis.* **66**, 2180–2183 (2019).
18. Y.-W. Huang *et al*., Origin, evolution, and genotyping of emergent porcine epidemic diarrhea virus strains in the United States. *mBio* **4**, e00737-13 (2013).
19. C.-M. Lin, L. J. Saif, D. Marthaler, Q. Wang, Evolution, antigenicity and pathogenicity of global porcine epidemic diarrhea virus strains. *Virus Res.* **226**, 20–39 (2016).
20. B. Yount *et al*., Reverse genetics with a full-length infectious cDNA of severe acute respiratory syndrome coronavirus. *Proc. Natl. Acad. Sci. U.S.A.* **100**, 12995–13000 (2003).
21. T. Scobey *et al*., Reverse genetics with a full-length infectious cDNA of the Middle East respiratory syndrome coronavirus. *Proc. Natl. Acad. Sci. U.S.A.* **110**, 16157–16162 (2013).
22. B. Yount, M. R. Denison, S. R. Weiss, R. S. Baric, Systematic assembly of a full-length infectious cDNA of mouse hepatitis virus strain A59. *J. Virol.* **76**, 11065–11078 (2002).
23. E. F. Donaldson *et al*., Systematic assembly of a full-length infectious clone of human coronavirus NL63. *J. Virol.* **82**, 11948–11957 (2008).
24. B. Yount, K. M. Curtis, R. S. Baric, Strategy for systematic assembly of large RNA and DNA genomes: Transmissible gastroenteritis virus model. *J. Virol.* **74**, 10600–10611 (2000).
25. V. D. Menachery *et al*., Trypsin treatment unlocks barrier for zoonotic bat coronavirus infection. *J. Virol.* **94**, e01774-19 (2020).
26. A. Beall *et al*., Characterization of a pathogenic full-length cDNA clone and transmission model for porcine Epidemic diarrhea virus strain PC22A. *mBio* **7**, e01451-15 (2016).
27. J. Huynh *et al*., Evidence supporting a zoonotic origin of human coronavirus strain NL63. *J. Virol.* **86**, 12816–12825 (2012).
28. S. Agnihothram *et al*., Development of a broadly accessible Venezuelan equine encephalitis virus replicon particle vaccine platform. *J. Virol.* **92**, e00027-18 (2018).
29. Y. L. Yang *et al*., Broad cross-species infection of cultured cells by bat HKU2-related swine acute diarrhea syndrome coronavirus and identification of its replication in murine dendritic cells in vivo highlight its potential for diverse interspecies transmission. *J. Virol.* **93**, e01448-19 (2019).
30. J. Y. Baik, K. H. Lee, A framework to quantify karyotype variation associated with CHO cell line instability at a single-cell level. *Biotechnol. Bioeng.* **114**, 1045–1053 (2017).
31. G. Jiang *et al*., Comprehensive comparison of molecular portraits between cell lines and tumors in breast cancer. *BMC Genomics* **17** (suppl. 7), 525 (2016).
32. S. Vcelar *et al*., Karyotype variation of CHO host cell lines over time in culture characterized by chromosome counting and chromosome painting. *Biotechnol. Bioeng.* **115**, 165–173 (2018).
33. V. M. Corman *et al*., Link of a ubiquitous human coronavirus to dromedary camels. *Proc. Natl. Acad. Sci. U.S.A.* **113**, 9864–9869 (2016).
34. Y. J. Hou *et al*., SARS-CoV-2 reverse genetics reveals a variable infection gradient in the respiratory tract. *Cell* **182**, 429–446.e14 (2020).
35. E. Baudon *et al*., Swine influenza viruses in northern Vietnam in 2013-2014. *Emerg. Microbes Infect.* **7**, 123 (2018).
36. M. C. Niederwerder, R. A. Hesse, Swine enteric coronavirus disease: A review of 4 years with porcine epidemic diarrhoea virus and porcine deltacoronavirus in the United States and Canada. *Transbound. Emerg. Dis.* **65**, 660–675 (2018).
37. V. Sharma, S. Kaushik, R. Kumar, J. P. Yadav, S. Kaushik, Emerging trends of Nipah virus: A review. *Rev. Med. Virol.* **29**, e2010 (2019).
38. I. Vojtek, P. Buchy, T. M. Doherty, B. Hoet, Would immunization be the same without cross-reactivity? *Vaccine* **37**, 539–549 (2019).
39. I. Gilchuk *et al*., Cross-neutralizing and protective human antibody specificities to poxvirus infections. *Cell* **167**, 684–694.e9 (2016).
40. J. S. Guy, J. J. Breslin, B. Breuhaus, S. Vivrette, L. G. Smith, Characterization of a coronavirus isolated from a diarrheic foal. *J. Clin. Microbiol.* **38**, 4523–4526 (2000).
41. G. J. Hatch *et al*., Assessment of the protective effect of Imvamune and Acam2000 vaccines against aerosolized monkeypox virus in cynomolgus macaques. *J. Virol.* **87**, 7805–7815 (2013).
42. M. Hoffmann *et al*., SARS-CoV-2 cell entry depends on ACE2 and TMPRSS2 and is blocked by a clinically proven protease inhibitor. *Cell* **181**, 271–280.e8 (2020).
43. L. Vijgen *et al*., Complete genomic sequence of human coronavirus OC43: Molecular clock analysis suggests a relatively recent zoonotic coronavirus transmission event. *J. Virol.* **79**, 1595–1604 (2005).
44. W. Li *et al*., Angiotensin-converting enzyme 2 is a functional receptor for the SARS coronavirus. *Nature* **426**, 450–454 (2003).
45. Q. Wang *et al*., Bat origins of MERS-CoV supported by bat coronavirus HKU4 usage of human receptor CD26. *Cell Host Microbe* **16**, 328–337 (2014).
46. W. Li *et al*., Broad receptor engagement of an emerging global coronavirus may potentiate its diverse cross-species transmissibility. *Proc. Natl. Acad. Sci. U.S.A.* **115**, E5135–E5143 (2018).
47. A. Bonavia, B. D. Zelus, D. E. Wentworth, P. J. Talbot, K. V. Holmes, Identification of a receptor-binding domain of the spike glycoprotein of human coronavirus HCoV-229E. *J. Virol.* **77**, 2530–2538 (2003).
48. V. S. Raj *et al*., Dipeptidyl peptidase 4 is a functional receptor for the emerging human coronavirus-EMC. *Nature* **495**, 251–254 (2013).
49. M. B. Frieman *et al*., SARS-CoV pathogenesis is regulated by a STAT1 dependent but a type I, II and III interferon receptor independent mechanism. *PLoS Pathog.* **6**, e1000849 (2010).
50. J. K. Roth-Cross, S. J. Bender, S. R. Weiss, Murine coronavirus mouse hepatitis virus is recognized by MDA5 and induces type I interferon in brain macrophages/microglia. *J. Virol.* **82**, 9829–9838 (2008).
51. J. W. Tang *et al*.; INSPIRE investigators, Global epidemiology of non-influenza RNA respiratory viruses: Data gaps and a growing need for surveillance. *Lancet Infect. Dis.* **17**, e320–e326 (2017).
52. R. Carrasco-Hernandez, R. Jácome, Y. López Vidal, S. Ponce de León, Are RNA viruses candidate agents for the next global pandemic? A review. *ILAR J.* **58**, 343–358 (2017).
53. B. Hu, X. Ge, L.-F. Wang, Z. Shi, Bat origin of human coronaviruses. *Virol. J.* **12**, 221 (2015).
54. Y. Tao *et al*., Surveillance of bat coronaviruses in Kenya identifies relatives of human coronaviruses NL63 and 229E and their recombination history. *J. Virol.* **91**, e01953-16 (2017).
55. V. M. Corman *et al*., Evidence for an ancestral association of human coronavirus 229E with bats. *J. Virol.* **89**, 11858–11870 (2015).
56. R. L. Graham, R. S. Baric, Recombination, reservoirs, and the modular spike: Mechanisms of coronavirus cross-species transmission. *J. Virol.* **84**, 3134–3146 (2010).
57. M. Cotten *et al*., Spread, circulation, and evolution of the Middle East respiratory syndrome coronavirus. *mBio* **5**, e01062-13 (2014).
58. D. Forni, R. Cagliani, M. Clerici, M. Sironi, Molecular evolution of human coronavirus genomes. *Trends Microbiol.* **25**, 35–48 (2017).
59. A. Latinne *et al*., Origin and cross-species transmission of bat coronaviruses in China. bioRxiv:10.1101/2020.05.31.116061 (31 May 2020).
60. Y.-L. Yang *et al*., Characterization of a novel bat-HKU2-like swine enteric alphacoronavirus (SeACoV) infection in cultured cells and development of a SeACoV infectious clone. *Virology* **536**, 110–118 (2019).
61. S. Mulangu *et al*.; PALM Writing Group; PALM Consortium Study Team, A randomized, controlled trial of Ebola virus disease therapeutics. *N. Engl. J. Med.* **381**, 2293–2303 (2019).
62. J. Grein *et al*., Compassionate use of remdesivir for patients with severe Covid-19. *N. Engl. J. Med.* **382**, 2327–2336 (2020).
63. T. P. Sheahan *et al*., An orally bioavailable broad-spectrum antiviral inhibits SARS-CoV-2 in human airway epithelial cell cultures and multiple coronaviruses in mice. *Sci. Transl. Med.* **12**, eabb5883 (2020).
64. M. L. Agostini *et al*., Coronavirus susceptibility to the antiviral remdesivir (GS-5734) is mediated by the viral polymerase and the proofreading exoribonuclease. *mBio* **9**, e00221-18 (2018).
65. A. J. Brown *et al*., Broad spectrum antiviral remdesivir inhibits human endemic and zoonotic deltacoronaviruses with a highly divergent RNA dependent RNA polymerase. *Antiviral Res.* **169**, 104541 (2019).
66. T. P. Sheahan *et al*., Broad-spectrum antiviral GS-5734 inhibits both epidemic and zoonotic coronaviruses. *Sci. Transl. Med.* **9**, eaal3653 (2017).
67. A. J. Pruijssers *et al*., Remdesivir inhibits SARS-CoV-2 in human lung cells and Chimeric SARS-CoV expressing the SARS-CoV-2 RNA polymerase in mice. *Cell Rep.* **32**, 107940 (2020).
68. T. P. Sheahan *et al*., Comparative therapeutic efficacy of remdesivir and combination lopinavir, ritonavir, and interferon beta against MERS-CoV. *Nat. Commun.* **11**, 222 (2020).
69. D. Wang, L. Fang, S. Xiao, Porcine epidemic diarrhea in China. *Virus Res.* **226**, 7–13 (2016).
70. P. L. Paarlberg, A. H. Seitzinger, J. G. Lee, K. Mathews, *Economic Impacts of Foreign Animal Disease*, (Economic Research Service ERR-57, U.S. Department of Agriculture, 2008).
71. J. F. Drexler *et al*., Genomic characterization of severe acute respiratory syndrome-related coronavirus in European bats and classification of coronaviruses based on partial RNA-dependent RNA polymerase gene sequences. *J. Virol.* **84**, 11336–11349 (2010).
72. L. Du *et al*., The spike protein of SARS-CoV—A target for vaccine and therapeutic development. *Nat. Rev. Microbiol.* **7**, 226–236 (2009).
73. H. Kim, Y. K. Lee, S. C. Kang, B. K. Han, K. M. Choi, Recent vaccine technology in industrial animals. *Clin. Exp. Vaccine Res.* **5**, 12–18 (2016).
74. J. Zhao *et al*., Airway memory CD4(+) T cells mediate protective immunity against emerging respiratory coronaviruses. *Immunity* **44**, 1379–1391 (2016).
75. F. Li, Structure, function, and evolution of coronavirus spike proteins. *Annu. Rev. Virol.* **3**, 237–261 (2016).
76. C. Liu *et al*., Cell entry of porcine epidemic diarrhea coronavirus is activated by lysosomal proteases. *J. Biol. Chem.* **291**, 24779–24786 (2016).
77. Y. Yang *et al*., Receptor usage and cell entry of bat coronavirus HKU4 provide insight into bat-to-human transmission of MERS coronavirus. *Proc. Natl. Acad. Sci. U.S.A.* **111**, 12516–12521 (2014).
78. Y. Zheng *et al*., Lysosomal proteases are a determinant of coronavirus tropism. *J. Virol.* **92**, e01504-18 (2018).
79. E. S. White, Lung extracellular matrix and fibroblast function. *Ann. Am. Thorac. Soc.* **12** (suppl. 1), S30–S33 (2015).
80. J. Aman, E. M. Weijers, G. P. van Nieuw Amerongen, A. B. Malik, V. W. van Hinsbergh, Using cultured endothelial cells to study endothelial barrier dysfunction: Challenges and opportunities. *Am. J. Physiol. Lung Cell. Mol. Physiol.* **311**, L453–L466 (2016).

81. Y. L. Yang, J. Q. Yu, Y. W. Huang, Swine enteric alphacoronavirus (swine acute diarrhea syndrome coronavirus): An update three years after its discovery. *Virus Res.* **285**, 198024 (2020).
82. H. Amuguni, W. Bikaako, I. Naigaga, W. Bazeyo, Building a framework for the design and implementation of One Health curricula in East and Central Africa: OHCEAs One Health training modules development process. *One Health* **7**, 100073 (2019).
83. S. E. Baum, C. Machalaba, P. Daszak, R. H. Salerno, W. B. Karesh, Evaluating One Health: Are we demonstrating effectiveness? *One Health* **3**, 5–10 (2016).
84. T. Sheahan, B. Rockx, E. Donaldson, D. Corti, R. Baric, Pathways of cross-species transmission of synthetically reconstructed zoonotic severe acute respiratory syndrome coronavirus. *J. Virol.* **82**, 8721–8732 (2008).
85. A. C. Sims *et al*., Release of severe acute respiratory syndrome coronavirus nuclear import block enhances host transcription in human lung cells. *J. Virol.* **87**, 3885–3902 (2013).
86. M. L. Fulcher, S. H. Randell, Human nasal and tracheo-bronchial respiratory epithelial cell culture. *Methods Mol. Biol.* **945**, 109–121 (2013).
87. Y. Wang *et al*., Self-renewing monolayer of primary colonic or rectal epithelial cells. *Cell. Mol. Gastroenterol. Hepatol.* **4**, 165–182.e7 (2017).
88. K. Debbink, Human norovirus detection and production, quantification, and storage of virus-like particles human norovirus virus-like particles. *Curr. Protoc. Microbiol.* **31**, 15K.1.1-15K.1.45 (2013).
89. S. Agnihothram *et al*., A mouse model for betacoronavirus subgroup 2c using a bat coronavirus strain HKU5 variant. *mBio* **5**, e00047-14 (2014).
90. C. E. Edwards *et al*, Mutant Swine acute diarrhea syndrome coronavirus strain icSADS, complete genome. GenBank, https://www.ncbi.nlm.nih.gov/nuccore/MT039231. Deposited on 10 June 2020.
91. C. E. Edwards *et al*, Mutant Swine acute diarrhea syndrome coronavirus strain icSADS-tRFP, complete genome. GenBank, https://www.ncbi.nlm.nih.gov/nuccore/MT039232. Deposited on 10 June 2020.